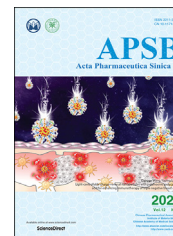




Chinese Pharmaceutical Association
Institute of Materia Medica, Chinese Academy of Medical Sciences

Acta Pharmaceutica Sinica B

www.elsevier.com/locate/apsb
www.sciencedirect.com



ORIGINAL ARTICLE

Discovery of novel 4-phenylquinazoline-based BRD4 inhibitors for cardiac fibrosis



Zhangxu He^{a,†}, Haomiao Jiao^{a,†}, Qi An^a, Xin Zhang^a,
Dan Zengyangzong^a, Jiale Xu^a, Hongmin Liu^a, Liying Ma^{a,b,*},
Wen Zhao^{a,*}

^aState Key Laboratory of Esophageal Cancer Prevention and Treatment, Key Laboratory of Advanced Pharmaceutical Technology, Ministry of Education of China, School of Pharmaceutical Sciences, Zhengzhou University, Zhengzhou 450001, China

^bChina Meheco Topfond Pharmaceutical Co., Zhumadian 463000, China

Received 18 March 2021; received in revised form 27 June 2021; accepted 14 July 2021

KEY WORDS

BRD4;
Inhibitor;
4-Phenylquinazoline;
Cardiac fibrosis

Abstract Bromodomain containing protein 4 (BRD4), as an epigenetic reader, can specifically bind to the acetyl lysine residues of histones and has emerged as an attractive therapeutic target for various diseases, including cancer, cardiac remodeling and heart failure. Herein, we described the discovery of hit 5 bearing 4-phenylquinazoline skeleton through a high-throughput virtual screen using 2,003,400 compound library (enamine). Then, structure–activity relationship (SAR) study was performed and 47 new 4-phenylquinazoline derivatives toward BRD4 were further designed, synthesized and evaluated, using HTRF assay set up in our lab. Eventually, we identified compound C-34, which possessed better pharmacokinetic and physicochemical properties as well as lower cytotoxicity against NRCF and NRCM cells, compared to the positive control JQ1. Using computer-based molecular docking and cellular thermal shift assay, we further verified that C-34 could target BRD4 at molecular and cellular levels. Furthermore, treatment with C-34 effectively alleviated fibroblast activation *in vitro* and cardiac fibrosis *in vivo*, which was correlated with the decreased expression of BRD4 downstream target c-MYC as well as the depressed TGF- β 1/Smad2/3 signaling pathway. Taken together, our findings indicate that novel BRD4 inhibitor C-34 tethering a 4-phenylquinazoline scaffold can serve as a lead compound for further development to treat fibrotic cardiovascular disease.

© 2022 Chinese Pharmaceutical Association and Institute of Materia Medica, Chinese Academy of Medical Sciences. Production and hosting by Elsevier B.V. This is an open access article under the CC BY-NC-ND license (<http://creativecommons.org/licenses/by-nc-nd/4.0/>).

*Corresponding authors. Tel./fax: +86 371 67739546.

E-mail addresses: maliying@zzu.edu.cn (Liying Ma), zhaowen100@139.com (Wen Zhao).

[†]These authors made equal contributions to this work.

Peer review under responsibility of Chinese Pharmaceutical Association and Institute of Materia Medica, Chinese Academy of Medical Sciences.

<https://doi.org/10.1016/j.apsb.2021.07.018>

2211-3835 © 2022 Chinese Pharmaceutical Association and Institute of Materia Medica, Chinese Academy of Medical Sciences. Production and hosting by Elsevier B.V. This is an open access article under the CC BY-NC-ND license (<http://creativecommons.org/licenses/by-nc-nd/4.0/>).

1. Introduction

The bromodomain and extraterminal (BET) family, including BRD2, BRD3, BRD4 and BRDT, can recognize *N*-acetyl lysine post-translational modifications on histone tails, each of which contains two conserved bromodomains named BD1 and BD2^{1–3}. BD1 is mainly regarded as a chromatin-binding module and BD2 is typically used for transcription factor recruitment^{4,5}. Among the BET family, BRD4 is extensively explored and associated with various pathologic states, such as cancers, inflammation and cardiovascular diseases^{6–9}.

There are over 40 clinical trials of BRD4 inhibition, most of them are used for malignant tumors and leukemia^{3,10–12}. However, the occurrence of side effects, modest clinical efficacy and preclinical resistance have partly limited clinical application of BRD4 inhibitors^{3,13}. Therefore, there remains scope for the development of highly specific BRD4 inhibitors with alternative physicochemical, pharmacokinetic and pharmacodynamic profiles. Recent years, many types of BRD4 inhibitors have been generated (Fig. 1). GSK778 was found as a BD1 selective inhibitor with 130 times higher affinity for BD1 than BD2⁵. The BD2 selective inhibitor RVX-208 could significantly decrease atherosclerosis in hyperlipidemic apolipoprotein E-deficient mice¹⁴, and increase high-density lipoprotein cholesterol as well as apolipoprotein A-1 in monkeys¹⁵. The BRD4-selective inhibitor ZL0420 reveals evidently inhibitory activity toward BRD4 over other BET family members¹⁶. Based on rational drug design, Xiong's group¹⁷ discovered a bromodomain and kinase dual inhibitor P40, which displayed strongly antiproliferative activities against a small cancer cell panel. Also, BRD4 degrader QCA570 indicates complete and long-lasting tumor regression at 5 mg/kg against MV4-11 and RS411 acute leukemia xenograft models without apparent toxicity¹⁸.

BRD4 inhibition has been played a crucial role in relieving pathological cardiac hypertrophy^{19,20}, cardiac remodeling²¹, heart failure²¹, atherosclerosis¹⁴ and fibrosis^{22,23}. Research and development of BRD4 inhibitors and its underlying mechanism exploration in cardiovascular diseases have become a hot spot^{24,25}.

Cardiac fibrosis is a major global health problem related to almost all types of heart disease²⁶, which is featured by fibroblast overproliferation and reduction or conservation of collagen degradation, thus contributing to both systolic and diastolic dysfunction^{27–29}. To date, no targeted drugs have been approved for the treatment of cardiac fibrosis³⁰. JQ1, as the first reported BRD4 inhibitor, has been broadly used for exploring pharmacological functions of BRD4 and presents potential effect on treatment of cardiovascular diseases^{30–32}. For example, JQ1 treatment inhibited cardiac fibrosis and improved cardiac function in an STZ-induced diabetic mouse model³¹. However, JQ1's suboptimal pharmacokinetic properties *in vivo* has partly limited its clinical application²⁴. In addition to JQ1, few BRD4 inhibitors have been investigated for cardiac fibrosis. Although RVX-208 and I-BET762 (Fig. 1) are undergoing several clinical trials for cardiovascular diseases, such as atherosclerosis and dyslipidemia^{10,14,33}, their effects on reducing cardiac fibrosis, to our knowledge, have not been reported. Thus, development of more effective BRD4 inhibitors with druglike properties is urgently needed, which not only enriches the chemotypes, but also can provide new possibility to investigate BRD4's functions in cardiovascular diseases.

In the current study, a high-throughput virtual screen was conducted toward BRD4, leading to the hit 5 with the IC₅₀ value of 18.122 μmol/L (Fig. 2). Subsequently, we performed the structure-based optimization and biological evaluation, resulting in a novel series of 4-phenylquinazoline derivatives as BRD4 inhibitors. Eventually, molecule 28 (C-34) was provided and displayed potential effect on relieving cardiac fibrosis.

2. Results and discussion

2.1. Structure–activity (SAR) relationship study

To discover novel BRD4 inhibitors, we performed a high-throughput virtual screen using the Enamine library of 2,003,400 compounds according to the workflow shown in

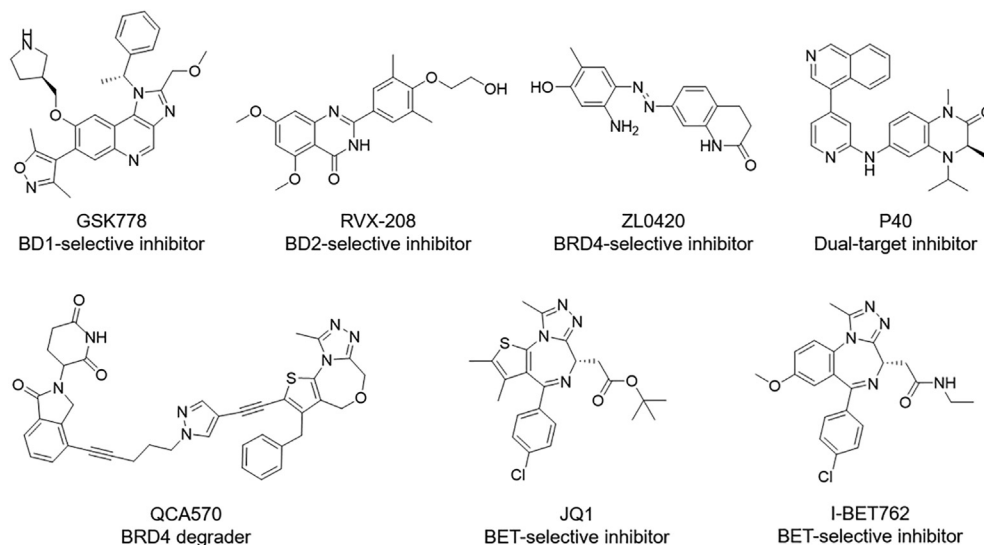


Figure 1 Representative structures of BRD4 inhibitors.

Fig. 3A. Briefly, compounds in the Enamine library were firstly washed and docked into the active site of BRD4 *via* rigid docking and flexible docking using MOE2019, resulting in 1000 molecules that were ranked according to the score of the best scored conformation. Next, an ADMET filtering procedure was applied to further exclude potentially problematic compounds in the 1000 molecules based on the rule-of-five (RO5) criteria, physico-chemical parameters and undesirable chemical features, yielding 350 molecules. Furthermore, the 350 molecules were clustered according to structural diversity and binding modes, which eventually provided 30 hits with different chemotypes. The 30 hits were then purchased from Topscience corporation and evaluated toward BRD4 using HTRF assay. Among these hits, 4-phenylquinazoline-based hit **5** binds to BRD4 with the IC_{50} value of 18.122 $\mu\text{mol/L}$ (**Fig. 3B**). The predicted binding modes indicate that the carbonyl oxygen of compound **5** binds in the acetyl-lysine binding site of BRD4 and interacts with the conserved residues Asn433 *via* a hydrogen bond with the distance of 2.3 Å (**Fig. 3C**). Additionally, the quinazoline moiety packs along the lipophilic surface defined by the WPF region. Besides, the 4-phenyl group in molecule **5** formed a water-mediated π -H interaction with Pro375.

Based on the binding modes, we firstly carried out the SAR study at R_2 , aiming to better target the acetyl-lysine binding site. As shown in **Table 1**, the replacement of the ester group in compound **5** with hydroxyl provided derivatives **6** and **7** with a slightly improved activity. Interestingly, changing the ester group to an amide group yielded analogue **8** with the IC_{50} value of 4.546 $\mu\text{mol/L}$, about 4-fold more potent than compound **5**. Next, derivatives **9–13** bearing a bigger substituent were synthesized, and the results showed that compounds tethering a heterocyclic group were less active than compounds with a phenyl group (**10 vs. 12**). Particularly, analogue **13** featuring a 4-aminobenzoic acid at R_2 revealed significantly binding affinity to BRD4(2) with the IC_{50} value of 3.045 $\mu\text{mol/L}$. Thus, we further focused on the effect of substituents of the benzene ring on potency, producing compounds **14–22**. Generally, compounds with a hydrophilic group on the benzene ring were superior to compounds bearing a hydrophobic group (**14 vs. 17, 16 vs. 19**). However, the electronic effect on activity seemed to be tolerated. No matter an electron-withdrawing or -donating group was introduced to the benzene ring of R_2 , the biological activity had not been improved (**15 vs. 16, 15 vs. 18**). To our delight, molecule **19** bearing a 4-sulfonamide displayed potent inhibitory activity ($IC_{50} = 1.530 \pm 0.185 \mu\text{mol/L}$), about 7-fold more active in comparison to compound **15** with no substituent. Additionally, conversion of the amino in compound **19** into a hydrophilic morpholine ring (**20**) reduced binding activity. Besides, the position of substituent on the benzene ring of R_2 was critical for activity with a relative order of $4 \geq 2 > 3$ -position (**19 vs. 21 vs. 22**) (**Tables 2 and 3**).

Considering the increased potency and our better SARs understanding, we next centered on the effects of R_1 and R_3 on activity. Comparing with analogue **19**, compound **25** featuring a 6-methyl group at R_1 suffered a significant activity loss with the IC_{50} value of 12.551 $\mu\text{mol/L}$. The similar result was also observed between molecules **33** and **34**. The docking study indicated that the introduction of methyl at R_1 into compound **33** might change the binding conformation, thus leading to weaker activity of compound **34** (Supporting Information **Fig. S1**). In addition, a survey of the position of substituent on the benzene ring at R_3 revealed that replacing 4-Cl with 2 or 3-Cl was detrimental for

binding affinity (**19 vs. 23 or 24**). Thus, various substituents were introduced to the 4-position of benzene ring at R_3 , and the results demonstrated that compounds with an electron-withdrawing group were more active than those with an electron-donating group (**26 vs. 33, 30 vs. 35**). Besides, derivatives tethering a hydrophobic substituent revealed more benefits on binding affinity (**33 vs. 35**). Compound **28** bearing a fluorine atom indicated the strongest inhibitory activity with the IC_{50} value of 0.242 $\mu\text{mol/L}$. However, the replacement of the fluorine atom with bigger substituents yielded compounds **37–42** without enhancing activity. Furthermore, adding an amino group into 4-position of compound **26** afforded analogue **52** with the IC_{50} value of 9.851 $\mu\text{mol/L}$, about a 6-fold decrease on potency, suggesting that the amino group was disfavored.

Encouraged by the above findings, the more detailed SARs study was conducted to explore the effect of substituents at R_2 . Compound **43** tethering a 4-carboxyaniline possessed the IC_{50} value of 0.925 $\mu\text{mol/L}$, more potent than derivative **45** bearing a 4-isopropylaniline ($IC_{50} = 5.269 \pm 0.367 \mu\text{mol/L}$). Changing the amino in **43** to aminomethyl provided molecule **44** with a slightly decreased activity. Also, in comparison to the promising compound **28**, derivatives **46** and **47** possessing a longer carbon chain revealed weaker binding affinity. Besides, conversion of sulfonyl into formyl resulted in decreased potency, indicating the sulfonyl as a contributor of activity (**49 vs. 50**). Eventually, a novel class of 4-phenylquinazoline-based BRD4 inhibitors was obtained *via* structure-based drug design. The summary for SARs analysis was displayed in **Fig. 4**. Next, we selected ten compounds with the IC_{50} values ranging from 0.2 to 2 $\mu\text{mol/L}$ to determine their binding affinity against BRD4 BD1. As shown in **Table 4**, most of them exhibited comparable inhibitory activity toward BRD4 BD1 and BD2, similar to the positive control JQ1. Subsequently, the ten derivatives were further evaluated their potency at the cellular level using isolated neonatal rat cardiac fibroblasts (NRCFs) and cardiac myocytes (NRCMs).

2.2. Chemistry

The synthesis of novel 4-phenylquinazoline derivatives was illustrated in **Scheme 1**. The intermediates **2a–b** were firstly obtained through cyclization of commercially available **1a–b** and urea in 71%–75% yields. Next, compounds **2a–b** were reacted with phosphorus oxychloride in the presence of *N,N*-diisopropylethylamine to provide compounds **3a–b** in 74%–76% yields³⁴, which, under nitrogen atmosphere, were coupled with appropriate phenylboronic acids, leading to the formation of intermediates **4a–p** in 35%–60% yields³⁵. Subsequently, raw materials **4a–p** were reacted with corresponding amines in diphenyl ether to give the desired compounds

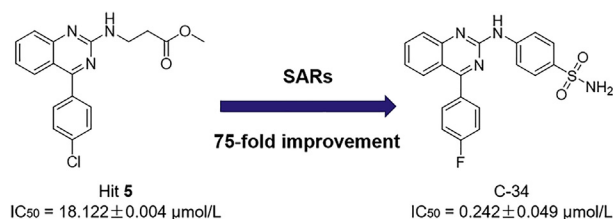


Figure 2 Discovery of potent 4-phenylquinazoline derivatives as BRD4 inhibitors.

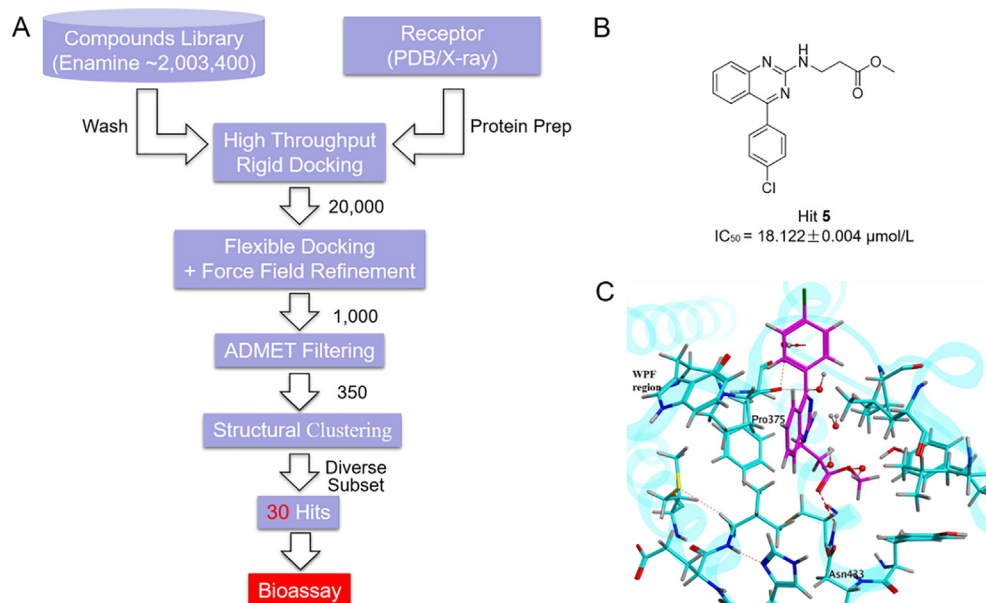


Figure 3 (A) Workflow of virtual screening. (B) The structure of hit 5. (C) The predicted binding modes of hit 5 (purple) with BRD4 BD2 (PDB code: 6C7Q).

Table 1 The structure–activity relationships of 4-phenylquinazoline derivatives 5–22.

Compd.	R ₂	BRD4(2) IC ₅₀ (μmol/L) ^a	Compd.	R ₂	BRD4(2) IC ₅₀ (μmol/L) ^a
5		18.122 ± 0.004	14		4.311 ± 0.180
6		8.314 ± 0.016	15		10.579 ± 0.367
7		12.388 ± 1.093	16		8.622 ± 0.164
8		4.546 ± 0.658	17		12.855 ± 0.947
9		14.789 ± 1.170	18		7.015 ± 0.517
10		13.300 ± 1.124	19		1.530 ± 0.185
11		9.037 ± 0.956	20		3.882 ± 0.589
12		7.048 ± 0.848	21		>20
13		3.045 ± 0.484	22		1.853 ± 0.268

^aThe IC₅₀ was calculated from HTRF assay. Data were expressed as the means ± SD, *n* = 3.

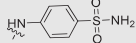
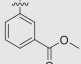
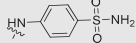
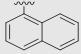
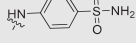
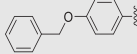
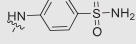
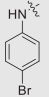
Table 2 The structure–activity relationships of 4-phenylquinazoline derivatives **23–42** and **52**.

The structure shows a quinazoline ring system with a phenyl group at the 4-position. Substituents are defined as: R₁ at the 6-position, R₂ at the 2-position, and R₃ at the 3-position.

Compd.	R ₁	R ₂	R ₃	BRD4(2) IC ₅₀ (μmol/L) ^a
19	H			1.530 ± 0.185
23	H			19.723 ± 1.295
24	H			15.130 ± 1.180
25	6-CH ₃			12.551 ± 0.307
26	H			1.629 ± 0.212
27	H			3.214 ± 0.206
28 (C-34)	H			0.242 ± 0.049
29	H			0.589 ± 0.052
30	H			0.688 ± 0.016
31	H			0.424 ± 0.038
32	H			10.268 ± 1.011
33	H			3.228 ± 0.089
34	6-CH ₃			13.608 ± 1.134
35	H			8.125 ± 0.084
36	H			9.908 ± 0.996
37	H			3.649 ± 0.562
38	H			5.168 ± 0.614
39	H			3.328 ± 0.522

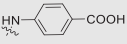
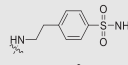
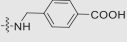
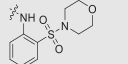
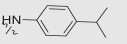
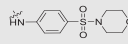
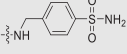
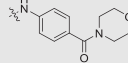
(continued on next page)

Table 2 (continued)

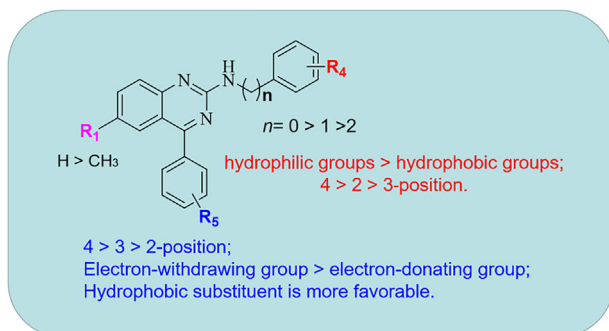
Compd.	R ₁	R ₂	R ₃	BRD4(2) IC ₅₀ (μmol/L) ^a
40	H			7.625 ± 0.882
41	H			4.762 ± 0.678
42	H			>20
52	H			9.851 ± 0.993

^aThe IC₅₀ was calculated from HTRF assay. Data were expressed as the means ± SD, *n* = 3.

Table 3 The SAR relationships of 4-phenylquinazoline derivatives 43–50.

Comp.	R ₂	BRD4(2) IC ₅₀ (μmol/L) ^a	Comp.	R ₂	BRD4(2) IC ₅₀ (μmol/L) ^a
43		0.925 ± 0.081	47 (C-34N)		18.629 ± 0.047
44		2.069 ± 0.625	48		6.689 ± 0.825
45		5.269 ± 0.367	49		1.334 ± 0.628
46		6.117 ± 0.258	50		3.069 ± 0.584

^aThe IC₅₀ was calculated from HTRF assay. Data were expressed as the means ± SD, *n* = 3.

**Figure 4** The summary for SARs study of the described compounds.

5–50 in 38%–66% yields. Besides, the intermediate **3a** was reacted with 4-bromoaniline in the presence of potassium carbonate to yield molecule **51** in 41% yield, which was further transformed into the title compound **52** in diphenyl ether in 51% yield.

Table 4 The inhibitory activity of representative compounds toward BRD4(1) and (2).

Compd.	IC ₅₀ (μmol/L) ^a	
	BRD4(1)	BRD4(2)
19	3.371 ± 0.528	1.530 ± 0.185
22	0.612 ± 0.214	1.853 ± 0.268
26	1.603 ± 0.205	1.629 ± 0.212
28 (C-34)	0.286 ± 0.046	0.242 ± 0.049
29	0.615 ± 0.127	0.589 ± 0.052
30	0.588 ± 0.024	0.688 ± 0.016
31	0.687 ± 0.054	0.424 ± 0.038
43	4.468 ± 0.361	0.925 ± 0.081
44	5.133 ± 0.626	2.069 ± 0.625
49	5.952 ± 0.248	1.334 ± 0.628
JQ1	0.122 ± 0.154	0.055 ± 0.015

^aThe IC₅₀ was calculated from HTRF assay. Data were expressed as the means ± SD, *n* = 3.

Table 5 The cytotoxicity of title compounds toward the tested cell lines.

Compd.	IC ₅₀ (μmol/L) ^a	
	NRCFs	NRCMs
C-34	48.213 ± 1.683	19.118 ± 1.400
JQ1	20.461 ± 1.351	4.526 ± 0.656

^aInhibitory activity was determined by exposure various concentrations of the tested compounds for 24 h to substance and expressed as concentration required to inhibit tested cell proliferation by 50% (IC₅₀). Data were presented as the means ± SD, *n* = 3. All experiments were carried out at least three independent times.

MOE2019³⁶. As shown in Fig. 6A and B, the sulfonamide oxygen of C-34 makes hydrogen bond interactions with Asn433 and Cys429, respectively. Additionally, we can observe that the phenyl group at R₂ forms a hydrophobic interaction with Val439. Besides, 4-phenylquinazoline moiety well occupies the hydrophobic WPF region, and the pyrimidine ring forms a π–π interaction with Trp374, which is important for BRD4 binding affinity³⁷. Overall, these results have well explained the capacity of compound C-34 on inhibiting BRD4(2).

2.5. Bromodomain selectivity of C-34 and its effect on increasing BRD4 stability in vitro

Bromodomains are conserved protein–protein interaction modules that are found in many proteins with different catalytic and scaffolding functions. They can recognize acetylated lysine by forming hydrogen bond interactions with the conserved asparagine residue³⁸. To confirm the selectivity profile, compound C-34 was evaluated toward 32 bromodomain-containing proteins using the commercial BROMOscan (DiscoverX) platform of Eurofins Co. at 1 μmol/L concentration (Fig. 7). We found that C-34 possessed relatively high selectivity toward BET family members, except for a moderate inhibitory activity against FALZ, CREBRP and EP300 (Details are provided in Supporting Information Table S1).

Next, cellular thermal shift assay (CETSA) was conducted in isolated NRCFs to confirm whether C-34 could target BRD4 at the cellular level with JQ1 as the positive control. As shown in Fig. 8A and B, the degradation of BRD4 began at 52 °C in DMSO treated cells. However, C-34 with the concentration of 10 μmol/L

could efficiently stabilize BRD4 from 43 to 61 °C, which was in close accordance with that obtained for JQ1. C-34N with a similar structure of C-34 and less BRD4 inhibitory activity was used as the negative control (IC₅₀ = 18.629 ± 0.047 μmol/L). We found that C-34N did not show similar stabilization on BRD4 compared with that in C-34. In addition, we observed that C-34 increased BRD4 thermal ability in a dose-dependent manner at 55 °C (Fig. 8C and D). These results indicated that C-34 could bind to BRD4 and enhance its thermal stabilization at the cellular level.

2.6. Effect of compound C-34 on Ang II-induced cardiac fibroblast activation

NRCFs, as the main cell type, synthesize and maintain extracellular matrix in heart tissue, which are the main determinant of

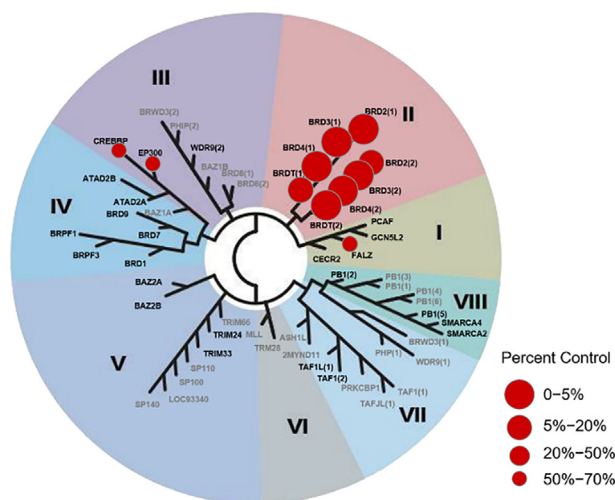


Figure 7 Selectivity evaluation of C-34 toward 32 BRD family members. The 32 tested BRDs are labeled in black, and the other BRDs are in gray. The results for primary screen binding interactions are reported as the “Percent Control”, with lower numbers indicating stronger hits in the matrix. The “Percent Control (%)” = [(Tested compound signal – Positive control signal)/(Negative control signal – Positive control signal)] × 100.

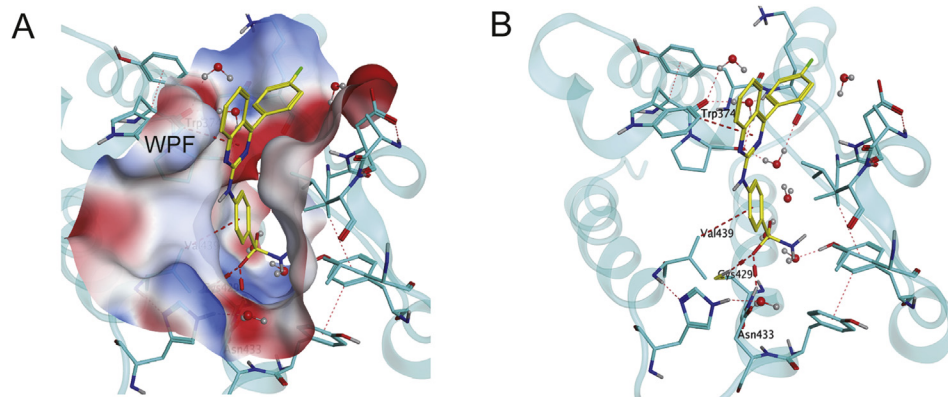


Figure 6 (A) The surface binding modes of molecule C-34 (yellow) to BRD4(2) (blue) (PDB code: 6C7Q). (B) The docking model of derivative C-34 (yellow) binds to BRD4(2) (blue). Water molecules are shown as red spheres.

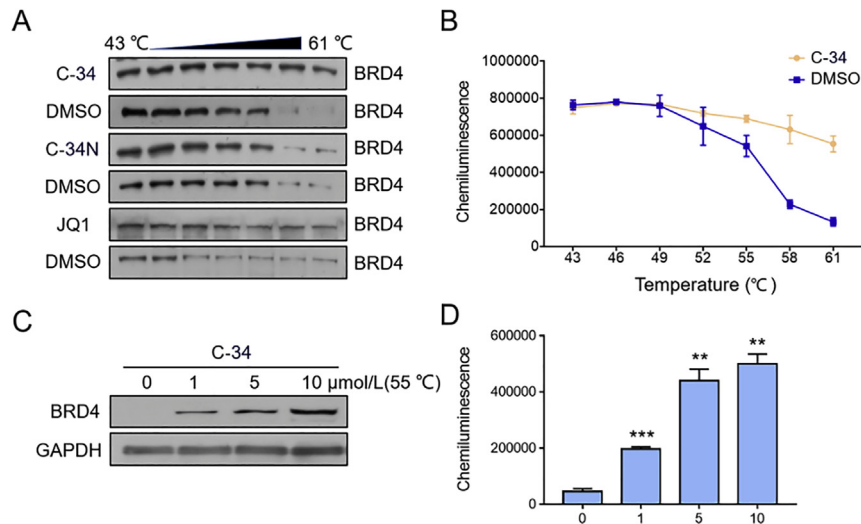


Figure 8 C-34 can effectively bind to BRD4 at the cellular level. (A) NRCFs were treated with 10 μmol/L C-34, C-34N or JQ1 for 4 h, respectively. Next, the cells were collected and heated from 43 to 61 °C. The Western blot analysis of BRD4 expression level. (C) NRCFs were pretreated with 0, 1, 5, 10 μmol/L C-34, and then heated at 55 °C. The Western blot analysis of BRD4 expression level. (B and D) The quantitative analysis of BRD4 expression level. Data were expressed as mean ± SD, $n = 3$. Three individual experiments were implemented for per group. ** $P < 0.01$, *** $P < 0.001$ vs. control.

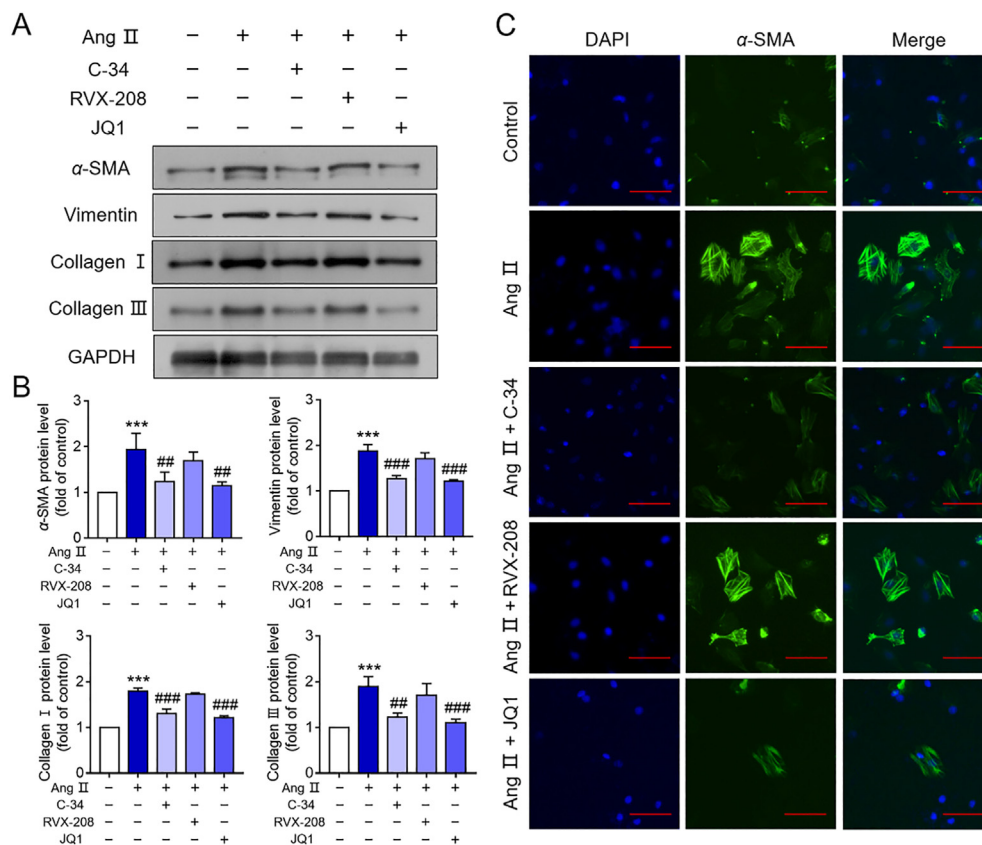


Figure 9 Compound C-34 can alleviate Ang II-induced cardiac fibroblast activation and collagen secretion *in vitro*. (A) The expression levels of α-SMA, vimentin, collagen I and III were determined by Western blot. (B) quantitative analysis of Western blot. (C) Immunofluorescent staining against α-SMA was performed in NRCFs, presence of compounds (C-34, JQ1 and RVX-208) or absence. Scale bar = 50 μm. The results were expressed as mean ± SD, $n = 3$. *** $P < 0.001$ vs. control, ## $P < 0.01$, ### $P < 0.001$ vs. Ang II group.

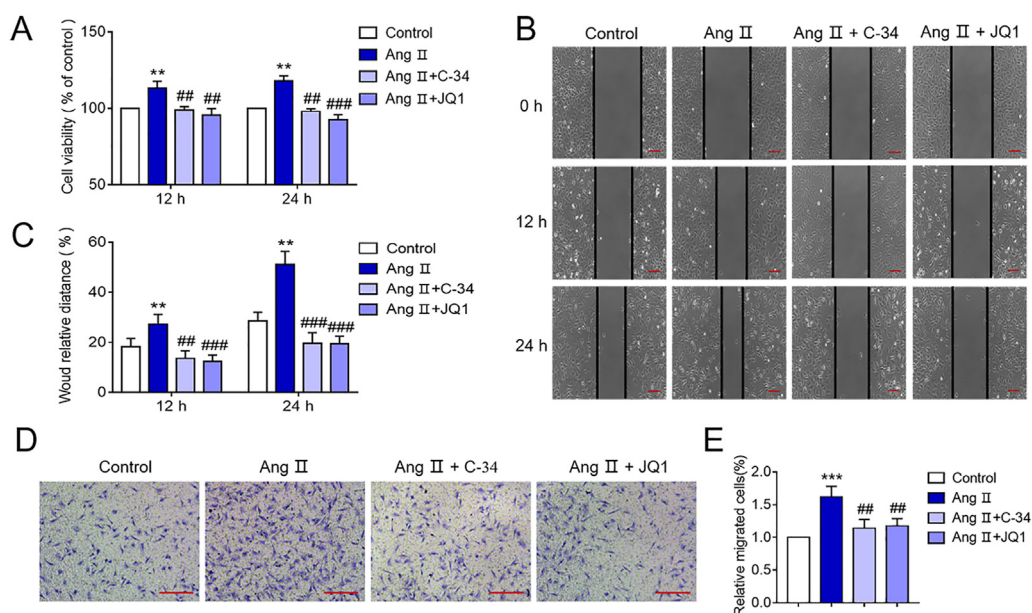


Figure 10 Compound C-34 suppressed Ang II-induced cardiac fibroblast proliferation and migration *in vitro*. Isolated NRCFs were incubated in the presence of serum-free medium containing C-34 (1 $\mu\text{mol/L}$), JQ1 (0.2 $\mu\text{mol/L}$) or absence for 1 h, and then stimulated with Ang II (10 $\mu\text{mol/L}$) for 12 or 24 h. (A) Cell proliferation was measured using MTT assay. Cell migration was measured by the (B) and (C) scratch test and (D) and (E) Transwell chamber assay. Data were represented as mean \pm SD, $n = 3$. Scale bar = 100 μm . Three individual experiments were carried out for per group. ** $P < 0.01$, *** $P < 0.001$ vs. control, ## $P < 0.01$, ### $P < 0.001$ vs. Ang II group.

cardiac fibrosis^{39,40}. To investigate the effect of C-34 on cardiac fibroblast activation *in vitro*, NRCFs were used to be treated by Angiotensin (Ang) II. JQ1 and RVX-208 were regarded as the positive control. As presented in Fig. 9A and B, after Ang II (10 $\mu\text{mol/L}$, 24 h) stimulation, the expression levels of α -SMA, vimentin, collagen I and III were significantly increased. Interestingly, the pretreatment of C-34 (1 $\mu\text{mol/L}$) effectively alleviated these abnormal changes, similar to those with JQ1. Using immunofluorescent staining, we found that Ang II stimulation obviously increased the fluorescence intensity (green) of α -SMA in cytosol, compared to that in the control group, whereas this effect was reversed by C-34 or JQ1 (Fig. 9C). In contrast, treatment with RVX-208 (a BD2 selective inhibitor) did not display any significantly effects on relieving cardiac fibroblast activation, compared to those of C-34 or JQ1.

2.7. Effect of C-34 on Ang II-induced cardiac fibroblast proliferation and migration *in vitro*

Ang II-induced cardiac fibroblast proliferation and migration contribute to cardiac fibrosis⁴¹. We could observe that pretreatment with C-34 or JQ1 markedly inhibited Ang II-induced cardiac fibroblast proliferation in 12 or 24 h (Fig. 10A). Also, wound scratch assay and transwell migration assay were conducted. As shown in Fig. 10B and C, the Ang II treated for 12 or 24 h evidently caused increased migration of NRCFs, compared to the control group, respectively. However, pretreatment with C-34 or JQ1 effectively inhibited the enhanced cell migration induced by Ang II. Similarly, pretreatment with C-34 could successfully suppress Ang II-induced NRCFs migration in the Transwell migration assay, similar to that with JQ1 (Fig. 10D and E). These results displayed that C-34 could indeed inhibit the proliferation and migration of NRCFs by Ang II.

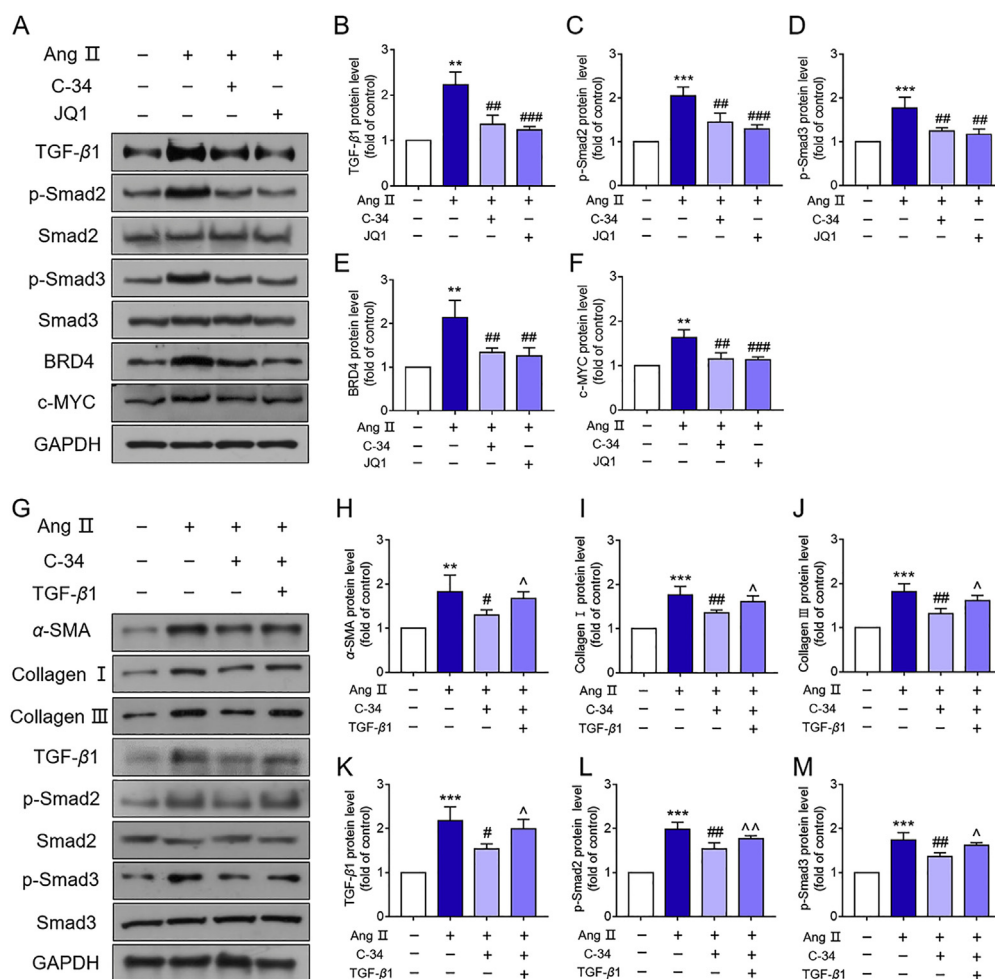
2.8. Compound C-34 can alleviate Ang II-induced activation of TGF- β 1/Smad2/3 signaling pathway in NRCFs

TGF- β 1/Smad2/3 signaling pathway is the primary mechanism of cardiac fibrosis^{42,43}. BRD4 was reported to be involved in TGF- β 1/Smad2/3 signaling pathway⁷. Our above findings prompted us to explore whether the potential mechanisms of C-34 on Ang II-induced cardiac fibroblast activation was through TGF- β 1/Smad2/3 signaling pathway. As presented in Fig. 11A–D, Ang II treatment caused an evident upregulation of TGF- β 1, p-Smad2 and p-Smad3 in comparison to the control group in NRCFs, which was associated with the upregulation of BRD4 and its downstream target c-MYC (Fig. 11E and F). However, pretreatment with C-34 effectively reversed Ang II-induced upregulation of TGF- β 1/Smad2/3 signaling pathway, which was related to the

Table 6 Pharmacokinetic properties of C-34 in rats^a.

PK parameter	iv (2 mg/kg)	po (10 mg/kg)
$t_{1/2}$ (h)	3.13	1.77
T_{max} (h)	—	2.67
C_{max} (ng/mL)	2820.9	2173.9
AUC_{last} (h \cdot ng/mL)	7100.0	15,298.7
$\text{AUC}_{\text{INF_pred}}$ (h \cdot ng/mL)	7127.2	15,393.7
MRT_{last} (h)	3.46	4.27
$V_{z_F_pred}$ (L/kg)	1.27	1.77
CL_{F_pred} (L/h/kg)	0.28	0.72
F (%)	—	43.10

^aRats ($n = 3$), data were represented as mean \pm SD; parameters were calculated from composite mean plasma concentration–time data.



downregulation of BRD4 and its downstream c-MYC by C-34. These effects were comparable to those by JQ1 treatment. Furthermore, we found that the therapeutic effect of C-34 could be blocked after TGF- β 1 co-treatment (Fig. 11G–M), as indicated by the increased expressions of α -SMA, collagen I, collagen III, TGF- β 1, p-Smad2 and p-Smad3, compared to those in C-34 treatment group. These findings exhibit that therapeutic effect of BRD4 inhibitor C-34 on Ang II-induced cardiac fibroblast activation is associated with downregulation of TGF- β 1/Smad2/3 signaling pathway.

Table 7 Physicochemical properties of C-34^a.

Compd.	MW	LogS	LogP	LogD	RB	HBA	HBD
C-34	394.0900	-4.685	3.827	2.626	4	6	2
JQ1	456.1387	-5.744	5.531	3.306	5	5	0

^aMW (molecular weight), logS (solubility), logP (distribution coefficient P), logD (distribution coefficient D at pH = 7.4), RB (rotatable bonds), HBA (hydrogen bond acceptors), HBD (hydrogen bond donors).

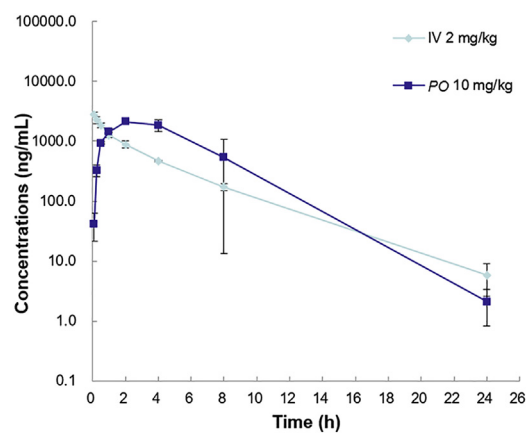


Figure 12 The plasma concentration–time curve of C-34 in male SD rat.

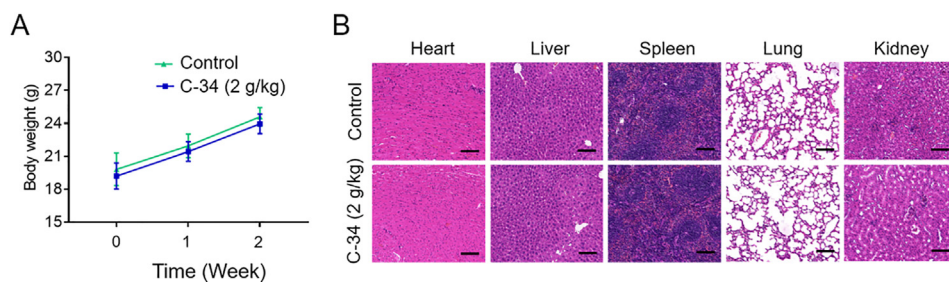


Figure 13 (A) The mice weight gain with intragastric administration of oil or C-34. (B) H&E staining of the main tissue sections from control and C-34 treated mice. $n = 10$ each group. Scale bar = 200 μm .

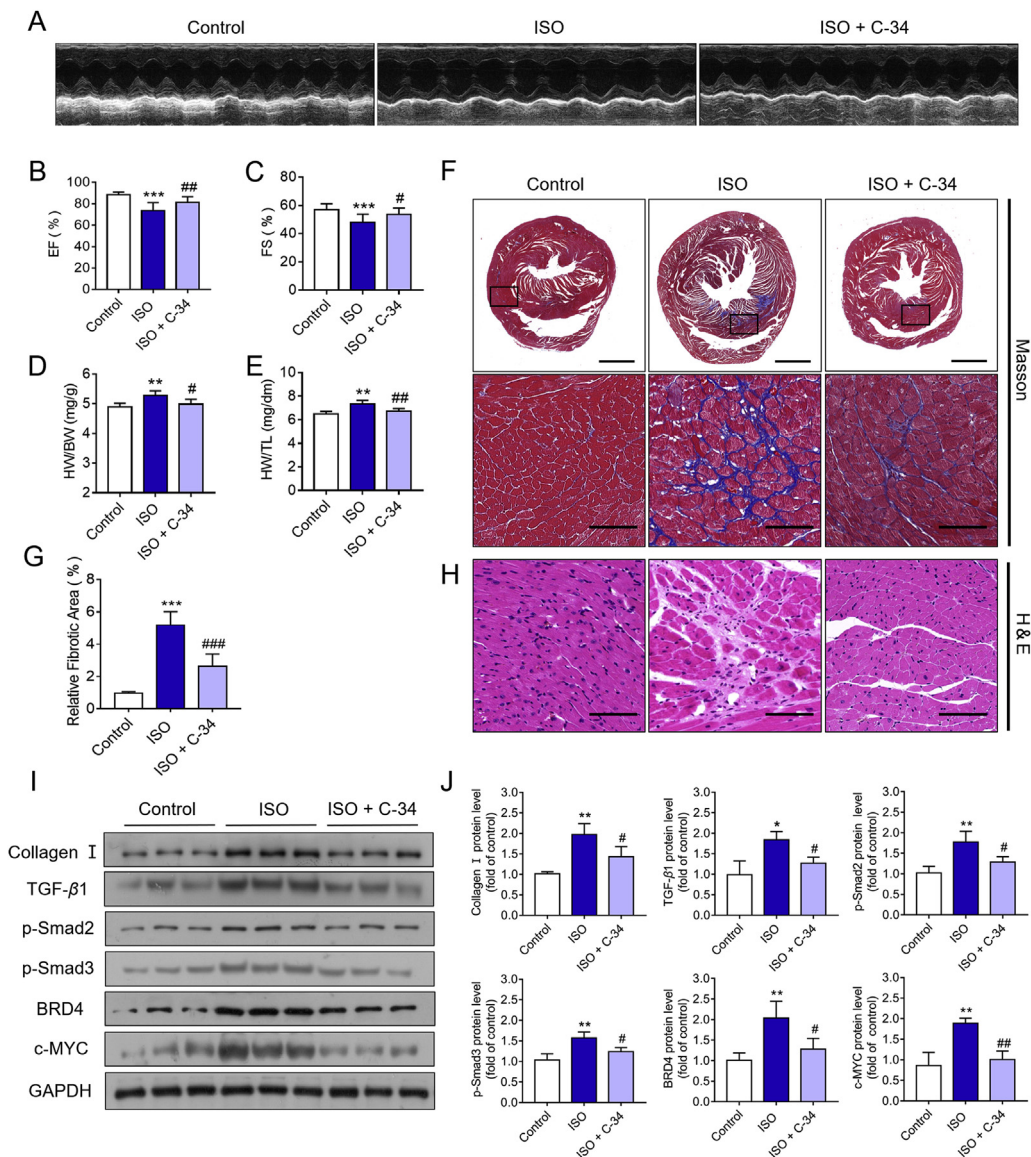


Figure 14 Effects of C-34 on ISO-induced pathological cardiac remodeling *in vivo*. (A) Representative traces of M-mode echocardiography were used to quantify ejection fraction. (B) EF%, ejection fraction. (C) FS%, fractional shortening. (D) HW/BW, ratio of heart weight to body weight. (E) HW/TL, ratio of heart weight to tibia length. (F) Masson trichrome staining from experimental mice's heart sections. Blue staining indicates fibrosis. Scale bar = 50 μm . (G) The quantitative results of relative fibrotic area by Image J software ($n = 5$ each group). (H) The images of HE staining ($n = 5$ each group). Scale bar = 50 μm . (I) and (J) The expression levels of collagen I, BRD4, c-MYC, TGF- β 1, p-Smad2 and p-Smad3 were measured by Western blot and quantitative analysis normalized to GAPDH ($n = 3$ each group). The dates were represented as mean \pm SD. * $P < 0.05$, ** $P < 0.01$, *** $P < 0.001$ vs. control group, # $P < 0.05$, ## $P < 0.01$, ### $P < 0.001$ vs. ISO group.

2.9. Pharmacokinetic and physicochemical properties of C-34

Inspired by the significant efficacy of C-34 *in vitro*, we next evaluated its pharmacokinetic properties *in vivo*. As shown in Fig. 12 and Table 6, C-34 possessed a C_{\max} of 2173.9 ng/mL and an AUC of 15,298.7 h·ng/mL with oral administration as well as exhibited reasonable oral bioavailability of 43.1%. Additionally, C-34 had a favorable half life (iv: 3.13 h, po: 1.77 h), which was better than those of JQ1 (iv: 0.9 h, po: 1.4 h)^{44,45}. Besides, the physicochemical properties of C-34 were calculated with ADMETlab (<http://www.openmolecules.org>). As shown in Table 7, C-34 revealed more favorable solubility and distribution coefficient than those of JQ1. Furthermore, C-34 obeyed all rule-of-five (RO5) criteria. These results displayed that C-34 possessed potential drug-like properties.

2.10. Safety evaluation of compound C-34 *in vivo*

The latent side effects of BRD4 inhibitors have partly limited their clinical application⁴⁶. Next, an acute toxicity test was performed to determine C-34's safety *in vivo*. The mice were not fed the night before; then, intragastric administration with a dose of 2 g/kg was carried out at one time. Subsequently, the mice were fed normally and frequently observed for 2 weeks. In this time, all mice with the treatment of C-34 survived and sustained their weight without obvious abnormalities (Fig. 13A). Additionally, compared with the control group, H&E staining confirmed that C-34 had no apparent toxicity in heart, liver, spleen, lung and kidney (Fig. 13B).

2.11. BRD4 inhibition with C-34 attenuates ISO-induced pathological cardiac remodeling *in vivo*

An isoprenaline (ISO)-induced pathological cardiac remodeling mice model⁴⁷ was established to explore the role of C-34 *in vivo*. As shown in Fig. 14A–H, ISO treatment (5 mg/kg/day) for 21 days resulted in significantly decreased cardiac contractile function, demonstrated by the decreased ejection fraction (EF%) and fractional shorting (FS%), the increased ratio of heart weight to body weight (HW/BW) and ratio of heart weight to tibia length (HW/TL), significant cardiac fibrosis (blue) and myocardial hypertrophy by Masson trichrome staining and HE staining. However, concomitant treatment with C-34 (20 mg/kg/day) effectively reversed ISO-induced impaired contractile function, cardiac hypertrophy and fibrosis.

Meanwhile, ISO treatment showed an obvious upregulation of collagen I, TGF- β 1, p-Smad2 and p-Smad3, compared with control group *in vivo*, which was linked to the upregulation of BRD4 and its downstream target c-MYC (Fig. 14I and J). Interestingly, C-34 successfully reversed ISO-induced upregulation of collagen I and TGF- β 1/Smad2/3 signaling pathway, which was associated with the downregulation of BRD4 and its downstream c-MYC. Overall, these results revealed that BRD4 inhibitor C-34 could effectively attenuate ISO-induced pathological cardiac fibrosis and thus improve cardiac function.

3. Conclusions

In the current study, we screened and reported the structure-based design, synthesis and biological evaluation of 47 BRD4 inhibitors

featuring a novel 4-phenylquinazoline scaffold. The promising molecule C-34 was identified *via* the detailed SARs exploration and exhibited effective BRD4 inhibitory activity. The binding modes of C-34 with BRD4 were verified not only by the molecular docking, but also by the cellular thermal shift assay. Besides, C-34 showed favorable pharmacokinetic and physicochemical properties as well as low cytotoxicity. More importantly, C-34 dramatically relieved fibroblast activation *in vitro* and cardiac fibrosis *in vivo*, which was linked to the decreased BRD4 activity, its downstream c-MYC expression and the depressed TGF- β 1/Smad2/3 signaling pathway. Overall, 4-phenylquinazoline derivative C-34, as a potent BRD4 inhibitor, can serve as a novel lead for further development to treat fibrotic cardiovascular disease.

4. Experimental

4.1. General procedures

Reagents and solvents were gained from standard suppliers and directly used. Melting points were determined on an X-5 micro-melting apparatus and were not corrected. Reactions were monitored by thin-layer chromatography (TLC) or liquid chromatography–mass spectrometry (LC–MS). TLC was performed on glass or aluminum-backed 60 silica plates coated with UV254 fluorescent indicator. ¹H and ¹³C NMR spectra were separately determined with a 400 and 100 MHz spectrometer. Mass spectra were obtained with the Waters Acquity UPLC instrument using positive electrospray. The products were detected as a summed UV wavelength of 210–350 nm. The spectra data of derivatives was offered in Supporting Information.

4.2. General procedure for the synthesis of compounds (2a–b)

A mixture of raw materials **1a–b** (20 mmol) and urea (200 mmol) was stirred at 140 °C for 5 h and then cooled to 100 °C. Water was added, and the precipitated solid was filtered off and washed three times with water to yield the crude product. The crude product was recrystallized from ethanol to provide the pure compounds **2a–b** as white solid.

4.3. General procedure for the synthesis of compounds (3a–b)

To a solution of **2a–b** (8 mmol) and phosphorus oxychloride (24 mmol) in 1,4-dioxane (25 mL) was added dropwise *N,N*-diisopropylethylamine (16 mmol) at 0 °C. Next, the reaction mixture was stirred and refluxed at 90 °C for 5 h before cooling to room temperature. Subsequently, the mixture was poured on crushed ice, and the precipitated solid was filtered off, washed with water, dried and recrystallized from ethanol to give compounds **3a–b** as white solid.

4.4. General procedure for the synthesis of compounds (4a–p)

A mixture of compounds **3a–b** (8 mmol), appropriate phenylboronic acids (7.2 mmol) and sodium carbonate (9.6 mmol) in 1,4-dioxane/water (12 mL, 5:1) were added tetrakis(triphenylphosphine)palladium (0.4 mmol). The mixture was stirred at 90 °C for 2–5 h under nitrogen atmosphere. Upon completion of the reaction indicated by TLC, the solvent was distilled off and extracted with ethyl acetate. The organics were dried and evaporated to dryness. Purification by

silica chromatography (PE/EA = 10:1) afforded intermediates **4a–p** as yellow solid.

4.5. General procedure for the synthesis of compounds (5–50)

To the solution of **4a–p** (2 mmol) in diphenyl ether (8 mL), suitable amines (4 mmol) were added. The resulting mixture was stirred at 150 °C for 4–8 h and then purified by flash column chromatography to provide **5–50** as yellow solid.

4.6. General procedure for the synthesis of compound (52)

To a well-stirred solution of compound **3a** (2 mmol) in ethanol (10 mL), 4-bromoaniline (1.8 mmol) and potassium carbonate (1.5 mmol) were added. The resulting mixture was stirred at room temperature for 3 h and then quenched with water and extracted with ethyl acetate. Subsequently, the combined organic phase was purified by flash column chromatography (PE/EA = 8:1) to yield **51** as a yellow solid. Following a similar procedure as compounds **5–50**, compound **52** was obtained as a yellow solid.

4.7. Molecular docking

The molecular docking study, including protein preparation, ligand preparation and docking simulation, was conducted using MOE 2019. The crystal structure of a molecule CF53 binding to BRD4(2) (PDB code: 6C7Q) was regarded as the docking receptor and prepared by adding missing atoms, removing waters and taking energy minimization using QuickPrep module. The three-dimensional structures of compounds **5** and C-34 were produced by taking energy minimization and conformational search. The protonation states of receptor protein and ligands were adjusted at $pK_a = 7$. Compounds **5** and C-34 then were docked into the binding pocket of BRD4(2). The 20 best-scored ligand–protein complexes of each ligand were kept for further analysis after the docking simulations.

4.8. HTRF assay

Compounds were evaluated by biochemical bromodomain binding assay. GST-BRD4, biotin-H4, anti-GST-cryptate, streptavidin-d2, compounds and detection buffer were presented in the 20 μ L system. After mixture incubation for 3 h, the fluorescence signal was detected by PerkinElmer Envision microplate reader equipped with 320 nm excitation and 620 and 665 nm emission. The results were analyzed by SPSS 20 and GraphPad Prism 7 software.

4.9. BROMOScan assay

BROMOScan bromodomain profiling was offered by DiscoverX Corp. (Fremont, CA, <http://www.discoverx.com>). The binding affinities of C-34 across 32 bromodomains were evaluated using the DiscoverRx BROMOScan platform of Eurofins Co. at 1 μ mol/L concentration. The results are reported as “% Ctrl” where lower numbers indicate stronger hits in the matrix.

4.10. Cell culture and treatment

All animal procedures and experiments were approved by the Ethical Committee of Zhengzhou University. The hearts of 1–3-day-old neonatal Sprague–Dawley rats were removed into the

prepared D-hank's buffer (pH = 7.18) to cut into the almost same sections. Then, all the sections were transferred into the trypsin buffer (0.8 mg/mL) at 4 °C overnight. The next day, these sections were digested in the collagenase type II buffer (0.8 mg/mL). Subsequently, the cells were collected in the complete medium and seeded into a 10 cm culture dish for 2 h. After that, neonatal rat cardiac fibroblasts (NRCFs) and neonatal rat cardiac myocytes (NRCMs) were separated and used in the following experiments.

4.11. MTT assay

MTT assay was utilized to measure the compounds' cytotoxicity and cell viability. NRCFs and NRCMs were seeded into the 96-well plate with an appropriate density, respectively. After the pretreatment of compounds, MTT was added into each well of plate with a solution of 5 mg/mL. After incubation for 4 h at 37 °C, the wells of MTT were replaced by 150 μ L DMSO. Finally, the plate was determined at 490 nm. All the results were analyzed by SPSS 20 software.

4.12. Western blot assay

Treated NRCFs were collected with lysis RIPA buffer by the procedure. BCA assay was utilized to detect the protein concentration. After that, proteins were separated by 10% SDS-PAGE and transferred to nitrocellulose membrane. All blots were blocked with 5% nonfat milk for 2 h, subsequently incubated with appropriate primary antibodies at 4 °C overnight. The next day, blots were incubated with secondary antibody (1: 10,000) for 2 h. Finally, the blots were washed 3 times with PBST, and then examined by chemiluminescence. All the data were measured and analyzed by Image J and GraphPad Prism 7 software.

4.13. Cellular thermal shift assay (CETSA)

Cellular thermal shift assay was used to evaluate the ability of compounds in binding to BRD4 in cells. Firstly, NRCFs were treated with no FBS media containing 10 μ mol/L JQ1, C-34, C-34N or 1% DMSO for 4 h, respectively. Then the treated cells were collected into 200 μ L tube and heated for 20 min from 43 to 61 °C. Dose-dependent assay: 1, 5, 10 μ mol/L C-34 or 1% DMSO was added into NRCFs for 4 h, respectively. After that, cells were heated for 20 min at 55 °C. Subsequently, the protein of treated cells was extracted and used for Western blot analysis.

4.14. Immunofluorescence

Treated NRCFs were fixed in 4% paraformaldehyde overnight, and then incubated in 0.1% Triton X-100 for 10 min and blocked in 5% BSA for another 20 min. Next, NRCFs were incubated with primary antibody (α -SMA 1:300) at 4 °C overnight. Subsequently, cells were washed 3 times with PBS and incubated with Alexa fluor® 488 Goat Anti-rabbit IgG (1: 200) for 2 h away from the light. After being washed 3 times with PBS, cells were incubated with DAPI for another 15 min. Finally, they were observed and photographed by laser confocal microscopy.

4.15. Wound scratch assay

Wound scratch assay was utilized to evaluate the cell migration ability. NRCFs were cultured in a 6-well plate. After the cells

density reached 90%–95%, a wound was scratched with a 200 μ L tip. Next, the medium was removed and added prepared medium with 2% FBS and compounds (C-34 and JQ1) for 24 h incubation. Subsequently, photographs were taken during the experiment.

4.16. Transwell assay

NRCFs were seeded into the upper of chamber of transwell plate with appropriate density. The upper chamber containing serum-free medium and bottom chamber containing complete medium were pretreated with compound C-34 or JQ1 for 1 h, respectively. Then, Ang II was added into the upper chamber. Cells were incubated at 37 °C for 24 h, fixed with pre-cooled methanol for 1 h and stained with crystal violet for 30 min. The results were photographed by an upright microscope. The number of invading cells were analyzed by Image J software.

4.17. In vivo pharmacokinetic study

The pharmacokinetic assay of C-34 were performed in male Sprague–Dawley rats. C-34 was firstly administered intravenously (iv) or orally (po) to male SD rats at a dose of 2 and 10 mg/kg separately. Then, blood samples were collected into heparinized eppendorf tubes at 0.083, 0.25, 0.5, 1, 2, 4, 8, 12, and 24 h. Subsequently, the intravenous injection plasma was separated from whole blood by centrifuging at 4 °C and 6000 rpm for 8 min. Finally, the plasma samples were analyzed by LC–MS.

4.18. Acute toxicity assay

8–10 weeks old ICR mice, weighing 18–20 g, were housed in a conditioned environment for 7 days before the experiment. Later, they were divided into the control group and treated compound C-34 group. Starvation treatment 12 h was performed in advance. Then, intragastric administration with a dose of 2 g/kg compound was carried out at one time. The control group was given equal oil. After that, the mice were fed normally and frequently observed for 2 weeks. Ultimately, the main organs, including heart, liver, spleen, lung and kidney were collected for further experiment.

4.19. Hematoxylin and eosin (H&E) staining

The main tissues of the ICR mice were fixed in 4% paraformaldehyde for 48 h. After that, the tissues were embedded in paraffin and sectioned as 5 μ mol/L thickness. The sections were deparaffinized in xylene and rehydrated in ethanol. Subsequently, hematoxylin and eosin were used to stain for further histological examination.

4.20. Masson trichrome staining

As above mentioned, 5 μ mol/L slices were stained in Weigert medium for 10 min. The sections were placed in Ponceau fuchsin acid for another 10 min after being washed, and then placed in 1% phosphomolybdic acid aqueous for 5 min. Subsequently, the sections were placed in aniline blue for 5 min. After being placed in 0.2% acetic acid aqueous for 2 min, the sections were permeabilized with xylene and fixed with neutral resin.

4.21. Mice model of cardiac fibrosis

Pathological cardiac fibrosis animal models were established by intraperitoneal injection of ISO (5 mg/kg/day) for 21 days. Thirty

male C57/BL/6 mice (8–10 weeks old, 18–22 g) were randomly divided into 3 groups ($n = 10$ each group): control group (0.5% CMC-Na), ISO group (5 mg/kg/day), C-34 treatment group (20 mg/kg/day). As for C-34 treatment group, intraperitoneal injection of C-34 (20 mg/kg/day) was pretreatment 1 h before ISO treatment.

4.22. Echocardiography and morphometric measurements

Cardiac function was assessed after 21 days using Vevo 2100 instrument (Visual Sonics). The chest surface of mice was shaved and then the mice were held in hand. The echocardiographic system was performed to calculate the ejection fraction (EF%) and fractional shortening (FS%). After that, the mice were anesthetized, and their hearts were quickly removed, weighed and used for other measurements.

4.23. Animals

Adult male C57/BL-6 mice weighing 18–22 g were purchased from Beijing Vital River Laboratory Animal Technology Co. Ltd., China [certificate no. SCXL (Jing) 2007-0001]. Standard care was provided to all mice. All protocols applied to the mice were approved and supervised by the Ethical Committee of Zhengzhou University and were in accordance with the Guide for the Care and Use of Laboratory Animals published by National Institute of Health (NIH). All efforts were conducted to minimize the animal suffering and the number of sacrificed animals based on the rule of the replacement, refinement or reduction.

4.24. Date and statistical analysis

Results were expressed as mean \pm SD. Multiple group comparison was analyzed by one-way ANOVA. The differences between two groups were analyzed by Student's *t*-test. $P < 0.05$ was considered to be statistically significant.

Acknowledgments

This work was supported by National Key Grant from Chinese Ministry of Science and Technology (2016YFA0501800 by Wen Zhao), National Natural Science Foundation of China (81870297 by Wen Zhao; 81703328 by Liying Ma) and Henan Scientific Innovation Talent Team, Department of Education (19IRTSTHN001 by Wen Zhao, China); China Postdoctoral Science Foundation (2020M672249 by Liying Ma); Natural Science Foundation of Henan Province (No. 212300410392 by Liying Ma, China).

Author contributions

Zhangxu He: investigation, writing – original draft, writing – review & editing conceptualization, methodology. Haomiao Jiao: investigation, writing – original draft, writing – review & editing. Qi An: validation, visualization, data curation. Xin Zhang: software, visualization. Dan Zengyangzong: formal analysis, visualization. Jiale Xu: Formal analysis. Hongmin Liu: resources, supervision. Liying Ma: conceptualization, methodology. Wen Zhao: supervision, funding acquisition, resources.

Conflicts of interest

The authors declare no conflicts of interests.

Appendix A. Supporting information

Supporting information to this article can be found online at <https://doi.org/10.1016/j.apsb.2021.07.018>.

References

- Christophe D, Justin EC, Lei Z, Cheng H, Aneel KA, Ming-Ming Z. Structure and ligand of a histone acetyltransferase bromodomain. *Nature* 1999;**399**:491–6.
- Wu SY, Chiang CM. The double bromodomain-containing chromatin adaptor Brd4 and transcriptional regulation. *J Biol Chem* 2007;**282**:13141–5.
- Tang P, Zhang J, Liu J, Chiang CM, Ouyang L. Targeting bromodomain and extraterminal proteins for drug discovery: from current progress to technological development. *J Med Chem* 2021;**65**:2419–35.
- Cheung KL, Zhang F, Jaganathan A, Sharma R, Zhang Q, Konuma T, et al. Distinct roles of Brd2 and Brd4 in potentiating the transcriptional program for Th17 cell differentiation. *Mol Cell* 2017;**65**:1068–80.
- Omer Gilan IR, Kathy K, Matthew JB, Miriam MY, Nicola RH, Enid YNL, et al. Selective targeting of BD1 and BD2 of the BET proteins in cancer and immunoinflammation. *Science* 2020;**368**:387–94.
- Li Y, Zhao J, Gutgesell LM, Shen Z, Ratia K, Dye K, et al. Novel pyrrolopyridone bromodomain and extra-terminal motif (BET) inhibitors effective in endocrine-resistant ER+ breast cancer with acquired resistance to fulvestrant and palbociclib. *J Med Chem* 2020;**63**:7186–210.
- Song S, Liu L, Yu Y, Zhang R, Li Y, Cao W, et al. Inhibition of BRD4 attenuates transverse aortic constriction- and TGF-beta-induced endothelial-mesenchymal transition and cardiac fibrosis. *J Mol Cell Cardiol* 2019;**127**:83–96.
- Loven J, Hoke HA, Lin CY, Lau A, Orlando DA, Vakoc CR, et al. Selective inhibition of tumor oncogenes by disruption of super-enhancers. *Cell* 2013;**153**:320–34.
- Zhang K, Xu Y. Suppressing BRD4 exhibits protective effects against vincristine-induced peripheral neuropathy by alleviating inflammation and oxidative stress. *Biochem Biophys Res Commun* 2020;**532**:271–9.
- Liu Z, Wang P, Chen H, Wold EA, Tian B, Brasier AR, et al. Drug discovery targeting bromodomain-containing protein 4. *J Med Chem* 2017;**60**:4533–58.
- Theodoulou NH, Tomkinson NC, Prinjha RK, Humphreys PG. Clinical progress and pharmacology of small molecule bromodomain inhibitors. *Curr Opin Chem Biol* 2016;**33**:58–66.
- Zhang M, Zhang Y, Song M, Xue X, Wang J, Wang C, et al. Structure-based discovery and optimization of benzo[d]isoxazole derivatives as potent and selective BET inhibitors for potential treatment of castration-resistant prostate cancer (CRPC). *J Med Chem* 2018;**61**:3037–58.
- Bechter O, Schoffski P. Make your best BET: the emerging role of BET inhibitor treatment in malignant tumors. *Pharmacol Ther* 2020;**208**:107479.
- Gilham D, Wasiak S, Tsujikawa LM, Halliday C, Norek K, Patel RG, et al. RVX-208, a BET-inhibitor for treating atherosclerotic cardiovascular disease, raises ApoA-I/HDL and represses pathways that contribute to cardiovascular disease. *Atherosclerosis* 2016;**247**:48–57.
- Bailey D, Jahagirdar R, Gordon A, Hafiane A, Campbell S, Chatur S, et al. RVX-208: a small molecule that increases apolipoprotein A-I and high-density lipoprotein cholesterol *in vitro* and *in vivo*. *J Am Coll Cardiol* 2010;**55**:2580–9.
- Liu Z, Tian B, Chen H, Wang P, Brasier AR, Zhou J. Discovery of potent and selective BRD4 inhibitors capable of blocking TLR3-induced acute airway inflammation. *Eur J Med Chem* 2018;**151**:450–61.
- Lv K, Chen W, Chen D, Mou J, Zhang H, Fan T, et al. Rational design and evaluation of 6-(pyrimidin-2-ylamino)-3,4-dihydroquinoxalin-2(1H)-ones as polypharmacological inhibitors of BET and kinases. *J Med Chem* 2020;**63**:9787–802.
- Qin C, Hu Y, Zhou B, Fernandez-Salas E, Yang CY, Liu L, et al. Discovery of QCA570 as an exceptionally potent and efficacious proteolysis targeting chimera (PROTAC) degrader of the bromodomain and extra-terminal (BET) proteins capable of inducing complete and durable tumor regression. *J Med Chem* 2018;**61**:6685–704.
- Spiltoir JI, Stratton MS, Cavasin MA, Demos-Davies K, Reid BG, Qi J, et al. BET acetyl-lysine binding proteins control pathological cardiac hypertrophy. *J Mol Cell Cardiol* 2013;**63**:175–9.
- Stratton MS, Lin CY, Anand P, Tatman PD, Ferguson BS, Wickers ST, et al. Signal-dependent recruitment of BRD4 to cardiomyocyte super-enhancers is suppressed by a microRNA. *Cell Rep* 2016;**16**:1366–78.
- Anand P, Brown JD, Lin CY, Qi J, Zhang R, Artero PC, et al. BET bromodomains mediate transcriptional pause release in heart failure. *Cell* 2013;**154**:569–82.
- Stratton MS, McKinsey TA. Epigenetic regulation of cardiac fibrosis. *J Mol Cell Cardiol* 2016;**92**:206–13.
- Stratton MS, Haldar SM, McKinsey TA. BRD4 inhibition for the treatment of pathological organ fibrosis. *F1000Res* 2017;**6**:F1000. Faculty Rev-1015.
- Soo YK, Xin Z, Gabriele GS, Francisco A, Thais ARR, Kristin MF, et al. Epigenetic reader BRD4 governs nucleus-encoded mitochondrial transcriptome to regulate cardiac function. *Circulation* 2020;**142**:2356–70.
- Kulikowski E, Rakai BD, Wong NCW. Inhibitors of bromodomain and extra-terminal proteins for treating multiple human diseases. *Med Res Rev* 2021;**41**:223–45.
- Travers JG, Kamal FA, Robbins J, Yutzey KE, Blaxall BC. Cardiac fibrosis: the fibroblast awakens. *Circ Res* 2016;**118**:1021–40.
- Kong P, Christia P, Frangogiannis NG. The pathogenesis of cardiac fibrosis. *Cell Mol Life Sci* 2014;**71**:549–74.
- Lewis KS, Butler J, Bauersachs J, Sandner P. The three-decade long journey in heart failure drug development. *Handb Exp Pharmacol* 2017;**243**:1–14.
- Patrick R, Adrian FH, Scott DS, Faiez Z. Heart failure drug treatment. *Lancet* 2019;**393**:1034–44.
- Stratton MS, Bagchi RA, Felisbino MB, Hirsch RA, Smith HE, Riching AS, et al. Dynamic chromatin targeting of BRD4 stimulates cardiac fibroblast activation. *Circ Res* 2019;**125**:662–77.
- Guo M, Wang HX, Chen WJ. BET-inhibition by JQ1 alleviates streptozotocin-induced diabetic cardiomyopathy. *Toxicol Appl Pharmacol* 2018;**352**:9–18.
- Duan Q, McMahon S, Anand P, Shah H, Thomas S, Salunga HT, et al. BET bromodomain inhibition suppresses innate inflammatory and profibrotic transcriptional networks in heart failure. *Sci Transl Med* 2017;**9**:eaah5084.
- Mirguet O, Gosmini R, Toum J, Clement CA, Barnathan M, Brusq JM, et al. Discovery of epigenetic regulator I-BET762: lead optimization to afford a clinical candidate inhibitor of the BET bromodomains. *J Med Chem* 2013;**56**:7501–15.
- Kumar S, Shakya N, Gupta S, Sarkar J, Sahu DP. Synthesis and biological evaluation of novel 4-(hetero) aryl-2-piperazino quinazolines as anti-leishmanial and anti-proliferative agents. *Bioorg Med Chem Lett* 2009;**19**:2542–5.
- Yokoyama K, Ishikawa N, Igarashi S, Kawano N, Masuda N, Hamaguchi W, et al. Potent and orally bioavailable CCR4 antagonists: synthesis and structure-activity relationship study of 2-aminoquinazolines. *Bioorg Med Chem* 2009;**17**:64–73.
- Zhao Y, Zhou B, Bai L, Liu L, Yang CY, Meagher JL, et al. Structure-based discovery of CF53 as a potent and orally bioavailable bromodomain and extra-terminal (BET) bromodomain inhibitor. *J Med Chem* 2018;**61**:6110–20.
- Romero FA, Taylor AM, Crawford TD, Tsui V, Cote A, Magnuson S. Disrupting acetyl-lysine recognition: progress in the development of bromodomain inhibitors. *J Med Chem* 2016;**59**:1271–98.

38. Hu J, Tian CQ, Damaneh MS, Li Y, Cao D, Lv K, et al. Structure-based discovery and development of a series of potent and selective bromodomain and extra-terminal protein inhibitors. *J Med Chem* 2019;**62**:8642–63.
39. van Nieuwenhoven FA, Turner NA. The role of cardiac fibroblasts in the transition from inflammation to fibrosis following myocardial infarction. *Vasc Pharmacol* 2013;**58**:182–8.
40. Khalil H, Kanisicak O, Vagnozzi RJ, Johansen AK, Maliken BD, Prasad V, et al. Cell-specific ablation of Hsp47 defines the collagen-producing cells in the injured heart. *JCI Insight* 2019;**4**: e128722.
41. Simoes e Silva AC, Silveira KD, Ferreira AJ, Teixeira MM. ACE2, angiotensin-(1-7) and mas receptor axis in inflammation and fibrosis. *Br J Pharmacol* 2013;**169**:477–92.
42. Meng XM, Nikolic-Paterson DJ, Lan HY. TGF-beta: the master regulator of fibrosis. *Nat Rev Nephrol* 2016;**12**:325–38.
43. Frangogiannis NG. Cardiac fibrosis: cell biological mechanisms, molecular pathways and therapeutic opportunities. *Mol Aspect Med* 2019;**65**:70–99.
44. Filippakopoulos P, Qi J, Picaud S, Shen Y, Smith WB, Fedorov O, et al. Selective inhibition of BET bromodomains. *Nature* 2010;**468**: 1067–73.
45. Li F, MacKenzie KR, Jain P, Santini C, Young DW, Matzuk MM. Metabolism of JQ1, an inhibitor of bromodomain and extra terminal bromodomain proteins, in human and mouse liver microsomes. *Biol Reprod* 2020;**103**:427–36.
46. Schooling CM, Zhao JV. How might bromodomain and extra-terminal (BET) inhibitors operate in cardiovascular disease?. *Am J Cardiovasc Drugs* 2019;**19**:107–11.
47. Hu H, Jiang M, Cao Y, Zhang Z, Jiang B, Tian F, et al. HuR regulates phospholamban expression in isoproterenol-induced cardiac remodeling. *Cardiovasc Res* 2020;**116**:944–55.